JP&M Engineering
Journal of Petroleum and Mining Engineering

Petrophysical Evaluation and Parameters Relations Investigation of Nubia Formation in October field, Gulf of Suez, Egypt.

Mohamed A.Kassab[a], Ali E.Abbas[b], Ihab A.Osman[b] and Ahmed A.Eid[b]
[a] Deptment of Exploration, Egyptian Petroleum Research Institute (EPRI), Cairo, Egypt.
[b.] Geological and geophysical engineering department,, Petroleum and mining engineering faculty, Suez university, Suez, Egypt

Corresponding author email: aeae4@pme.suezuni.edu.eg

Article Info

Received 6 Mar. 2024
Revised 30 Apr. 2024
Accepted 13 May 2024

Keywords

Formation Evaluation, Petrophysical Parameters, Relation Investigation, Nubia Formation, October Field, Gulf of Suez

Abstract

October Field is one of the most prolific and giant oil fields in Gulf of Suez. It has been decades producing since its exploration in the late seventies of the last century with hundreds of wells drilled.
Petrophysical parameters such as shale volume, porosity, permeability, net reservoir thickness, net pay thickness and the ratio between them are highly important in oil industry as it indicates the best intervals in the reservoir to perforate and produce. This study aims to reach a reasonable evaluation of these parameters by calculating them from conventional well logs (Gamma ray, density, neutron and sonic logs) as well as integration of core data obtained from routine core analysis of 4 wells: OCT-A2B, OCT-B8, OCT-B6, OCT-K5.
In light of the petrophysical characters for the Nubia reservoir, it shows good reservoir quality with porosity ranges from 13 to 16 percent and shale volume ranges from 18 to 20 percent. In addition, excellent pay thickness for the Nubia reservoir as it ranges from 74 to 96 percent and good oil saturation as it ranges from 36 to 47 percent. Empirical equations from plotting porosity versus permeability of routine core analysis is used to predict permeability in un-cored intervals, this method lead to low R2 correlation coefficient (0.03 in horizontal permeability and 0.21 in vertical permeability), this is due to different values of porosity from cores and logs due to different measurement conditions. In addition, information obtained of the possible direction trends of enhanced petrophysical parameters as loops with Northwest-Southeast of increasing porosity and decreasing shale volume were found. This indicates sweet spots for development opportunities for Nubia reservoir in October field.

Introduction

October Field is located in the north-central part of the Gulf of Suez, Egypt (EGPC, 1996), with latitude from 28° 48' 00'' N to 28° 53' 00'' N and longitude from 33° 03' 00'' E to 33° 08' 00'' E. October field was discovered in 1977, the GS 195-1 well (later renamed October A-1) was drilled to test a large, NW-trending, fault- bounded structure that had been identified from a 1976 regional seismic survey in the October area. The well October A-1 was targeting Nukhul as primary target and Nubia as secondary target. The October field, positioned approximately 25 kilometers to the north of the vast Belayim field, exhibits a structural configuration characterized by elongated faulted blocks. These faulted blocks align in a northwest-southeast trend and have a northeast dip. These pre-Miocene faulted blocks extend along the strike of the field for approximately 20 kilometers (Zahran, 1986; EGPC, 1996; Kassem et al., 2021; Khattab et al., 2023). Figure 1 shows the location map of the wells involved in this study.

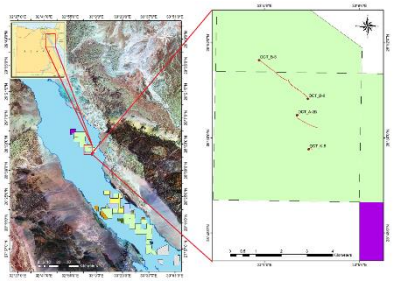

Figure 1 Location map of the study area, Gulf of Suez, Egypt (EGPC, 1996)

Nubia Formation is considered as a major reservoir in Gulf of Suez especially in October field. It contains around 1163 MMBO reserves. In spite of that Nubia has an attractive hydrocarbon potential (EGPC, 1996).

The current study aiming to evaluate the Nubia Formation in October field, Gulf of Suez, Egypt

calculating the volume of shale, porosity, saturation of water and thickness of net pay and the investigation of the porosity and permeability relations with the depth and versus one another after measuring these petrophysical parameters from core samples obtained from Nubia Formation.

Geological Setting

The Gulf of Suez region is a narrow water body situated in a North/Northwest-South/Southeast direction, serving as a natural division between the North-Eastern part of the African continent and the Sinai Peninsula. This region is part of the northern compartment of the Red Sea rift. The Gulf of Suez area holds significant importance in Egypt's exploration efforts and stands as the most extensively drilled and explored portion. It encompasses over 80 oil fields, hosting reservoirs ranging in age from the Precambrian period to the Quaternary period (Elsayed et al., 2021; El Nady et al., 2015). The Gulf of Suez basin is categorized into three distinct structural provinces, determined by the regional dip direction of its tilted fault blocks (Bosworth and McClay, 2001). The northern and southern provinces exhibit a southwestward dip, while the central province demonstrates a northeastward dip. Separation between both provinces occurs via two accommodation zones that trend in a northeast direction (Moustafa, 1976; Patton et al., 1994). With a length of approximately 320 kilometers and a width ranging from 60 to 25 kilometers, the Gulf of Suez Basin is classified as a rift basin. It is characterized by intricate tectonic activity, wherein faulted blocks are delineated by significant northwest-southeast faults (Clysmic direction), along with secondary southwest-northeast trending faults. This region is renowned as the most prolific oil rift basin in both the Middle East and Africa, boasting high levels of oil production (El Nady et al., 2015; Elsayed et al., 2021).

October Field is located in the north-central part of the Gulf of Suez, Egypt (EGPC,1996), with latitude from 28° 48' 00'' N to 28° 53' 00'' N and longitude from 33° 03' 00'' E to 33° 08' 00'' E. October field was discovered in 1977, the GS 195-1 well (later re-named October A-1) was drilled to test a large, NW-trending, fault- bounded structure that had been identified from a 1976 regional seismic survey in the October area. The October field, positioned approximately 25 kilometers to the north of the vast Belayim field, exhibits a structural configuration characterized by elongated faulted blocks. These faulted blocks align in a northwest-southeast trend and have a northeast dip. These pre-Miocene faulted blocks extend along the strike of the field for approximately 20 kilometers (Zahran, 1986; EGPC, 1996; Kassem et al., 2021; Khattab et al., 2023). The field is bounded to the west by a sequence of normal faults with downthrown displacement to the west, it is also divided into a main southern block and a secondary northern block (El-Ghamri et al., 2002; Radwan et al., 2021b).

The Miocene Nukhul Formation, which was produced from the onshore Abu Rudeis field, 10-15 km to the east, was the main objective, with the Paleozoic-Cretaceous Nubia sandstones as a secondary target (Lelek et al., 1992; Radwan et al., 2020). The Nukhul reservoir was absent, but the Nubia contained 541 ft of net oil pay, which tested 29.6 °API oil at 4562 Barrel Oil Per Day (BOPD). Logs showed a single Oil water Contact (OWC) at 11,670 ft True Vertical Depth Sub Sea (TVDSS) (Zahran, 1986). The wells were put on production in October 1977 (Zahran, 1986) and a production platform was installed in 1979 (Borling et al., 1996). The primary oil production at the October Field is derived from the sandstones within the Paleozoic-Cretaceous Nubia Formation (Lelek et al., 1992). In 1989, additional reserves were discovered in a smaller, separate Nubia pool with a shallower OWC in the North October Area by the discovery well, GS172-1 (October J-1), which penetrated Nubia-sandstones at 10,723 ft TVDSS and tested at a rate of 7880 BOPD from 254 ft of net oil pay. In the October field, the basal pre-rift reservoir section is primarily composed of various sandstones known as the "Nubian Sandstone". The Nubia Formation ranges in age from the Palaeozoic to the Lower Cretaceous and unconformably overlies the Precambrian crystalline basement and is conformably overlain by Upper Cretaceous shales of the Nezzazat Group (Hussein et al., 2017; Zahran, 1986). Figure 2 shows the litho-stratigraphic column of the October field (Peijs et al., 2012).

Deaf (2009) suggested that during the late Cretaceous period in the Gulf of Suez, there was a notable marine transgression, the lower part of the Gulf of Suez sequence, which is of the latest early Cretaceous age, appears to have been deposited in a continental basin. The late Cretaceous sedimentary record in the Gulf of Suez demonstrates a transition from continental alluvial deposits to marine carbonate sequences.

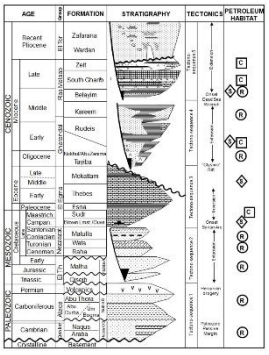

Figure 2 Tectonostratigraphic History and Stratigraphic Megasequences of Gulf of Suez (Peijs et al., 2012)

The Nubian Sandstone can be further subdivided into different groups based on lithological characteristics. The Lower Palaeozoic Qebliat Group, which corresponds to the previously used terms Nubia 'D' and 'C', is dominated by sandstone lithologies. The Carboniferous Ataqa Group, equivalent to the Nubia 'B' and the lower portion of the

Nubia 'A', consists of both dolomites and sandstones. This group exhibits a mixture of carbonate and siliciclastic facies. The Lower Cretaceous Malha Formation represents the upper part of the Nubia 'A' and is primarily composed of coarse-grained sandstones. These sandstones within the Malha Formation exhibit a coarser grain size compared to the other units.

Overall, the Nubian Sandstone in the October field comprises different lithological units, including the sandstone-dominated Lower Palaeozoic Qebliat Group, the dolomites and sandstones of the Carboniferous Ataqa Group, and the coarse-grained sandstones of the Lower Cretaceous Malha Formation. These sandstone units form the dominant reservoir section underlying the October field (Hasouba et al., 1992; El-Ghamri et al., 2002).

Materials and Methods

The data set available for the current study includes the complete set of logging data for four wells (OCT-A2B, OCT-B8, OCT-B6 and OCT-K5). The logging data includes Gamma ray (GR), Caliper (CALI) Deep and medium resistivity (RD and RM), Neutron (NPHI), Density (RHOB) and Sonic (DT). As for the core data, routine core analysis (RCAL) is available for all three cored wells (OCT-A2B, OCT-B8 and OCT-B6), while special core analysis (SCAL) is available for only two wells (OCT-A2B and OCT-B6). For the un-cored well OCT-K5, same set of logs is available except for the sonic log is missing in its dataset but it has Nuclear Magnetic Resonance log (NMR) available. Table 1 shows the detailed database used in current study.

Table 1 Detailed dataset

Well/ Data Type	GR	CALI	PEF	DRHO	RHOB/ NPHI	DT	RD	RM	NMR	RCAL	SCAL
OCT-A2B	√	√	×	√	√	√	√	√	×	√	√
OCT-B6	√	√	√	√	√	√	√	√	×	√	√
OCT-B8	√	√	√	√	√	√	√	√	×	√	×
OCT-K5	√	√	√	√	√	×	√	√	√	×	×

Formation evaluation for the studied wells

Well log data was used to perform formation evaluation to obtain petrophysical parameters like shale volume (Vsh), porosity (Ø), water saturation (Sw), reservoir, pay flags and the ratio between them. Shale volume is calculated by the linear formula (Eq.1) from gamma ray for a pessimistic estimation (Atlas, 1979) and from density-neutron log (Eq.2) (Schlumberger, 1972; Schlumberger, 2009). Porosity determination in the study is primarily obtained from density and neutron logs (Wyllie, 1963; (Asquith and Gibson, 1982; Schlumberger, 1972) (Eqs. 3 to 6). Water Saturation derived from Archie equation (Archie, 1942) (Eq.7) and from Indonesian equation (Poupon and Leveaux, 1971) (Eq.8). For reservoir and pay flags, standard cutoffs for shale volumes (50%), porosity (10%) and water saturation (50%) were applied in order and sequentially (Darling, 2005; Kassab et al., 2020; El-Din et al., 2013).

$$VSH=\frac{GR_{log}-GR_{sand}}{GR_{shale}-GR_{sand}} \text{ ----- (1)}$$

$$V_{sh}=\frac{X1-X0}{X2-X0} \text{ ---- (2)}$$

Where

$$X0 = NPHI_{ma}$$

$$X1=NPHI + M1(RHOB_{ma} - RHOB)$$

$$X2=NPHI_{sh} + M1\ (RHOB_{ma} - RHOB_{sh})$$

$$M_1=\frac{NPHI_{fl}-NPHI_{ma}}{RHOB_{fl}-RHOB_{ma}}$$

$$Ø=\frac{\rho_{ma}-\rho_{log}}{\rho_{ma}-\rho_{fluid}} \text{ ---- (3)}$$

Where:

Ø = formation porosity, fraction

ρ_ma = Density of the rock matrix, g/cm³

ρ_fluid = Density of saturation fluid, g/cm³

ρ_log = Density log reading (bulk density), g/cm³

$$Ø=\sqrt{\frac{Ø_N^2+Ø_D^2}{2}} \text{ ---- (4)}$$

$$\emptyset_e = \emptyset_t - \emptyset_{sh} V_{sh} \text{ ---- (5)}$$

$$\emptyset_{sh} = \frac{\rho_{ma} - \rho_{sh}}{\rho_{ma} - \rho_{fluid}} \text{ ---- (6)}$$

Where:

$\emptyset_e$= effective porosity, fraction

$\emptyset_t$= total porosity, fraction

$\emptyset_{sh}$= porosity of shale derived, fraction

V_{sh}= volume of shale at formation, fraction

$$S_W = \sqrt[n]{\frac{R_W}{\emptyset^m . R_T}} \text{ ---- (7)}$$

Where:

S_W= water saturation, fraction

$\emptyset$= porosity, fraction

R_W= resistivity of formation water, ohm.m

R_T= resistivity of uninvaded formation, ohm.m

m = cementation exponent

n = saturation exponent

$$SW_{indo} = \left\{ \frac{\sqrt{\frac{1}{Rt}}}{\left(\frac{Vsh^{(1-0.5Vsh)}}{\sqrt{Rsh}}\right) + \sqrt{\frac{\emptyset^m}{a.Rw}}} \right\}^{(2/n)} \text{ ---- (8)}$$

Where:

SW_{indo} = water saturation, fraction

Rt = resistivity of uninvaded formation, ohm.m

Rsh = resistivity of shale, ohm.m

Vsh =volume of shale, fraction

$\emptyset$ = porosity, fraction

a =Archie constant

R_w = resistivity of formation water, ohm.m

m = cementation exponent

Mapping of petrophysical parameters for lateral variation

After obtaining acceptable evaluation of petrophysical parameters on the level of wells. Mapping of these parameters is established for acquiring knowledge of lateral variation for these parameters especially the shale volume and porosity. The importance of this step is to identify any direction trends where the petrophysical parameters are enhanced for tracking development opportunities.

Petrophysical parameters relations investigation

After the tests of routine core analysis (RCAL) the results of porosity and permeability measured from the core plugs are plotted to investigate relations between each other and between these parameters and depth.

Results

Formation evaluation results

According to Kassab et al., 2024, wells OCT-A2B and OCT-B6 have core electric parameters obtained from special core analysis (SCAL) such as cementation exponent (m), saturation exponent (n), Archie constant (a), and the formation water resistivity (Rw). Table 2 shows the results of the SCAL regarding the core electric parameters.

Table 2 Core electric parameters resulted from SCAL

Well/Property	a	m	n	R_w
OCT-A2B	1	1.69	1.97	0.088
OCT-B6	1	1.63	1.72	0.07

Formation evaluation is performed to estimate shale volume (Vsh), porosity (Ø), water saturation (Sw), gross reservoir, net pay thicknesses, and net to gross ratio (N/G) for the Nubia Formation to all wells. Core electric parameters for the wells with those parameters were used. While assumed default values per the Gulf of Suez Petroleum Company (GUPCO) were used for the wells with no core electric properties measured (OCT-B8 and OCT-K5). The values used for cementation exponent (m), saturation exponent (n), Archie constant (a), and the formation water resistivity (Rw) are 1.95, 2, 1, and 0.016 respectively. Table 3 shows the results of the average formation evaluation parameters. Figure 3 shows the formation evaluation for well OCT-B8. Figure 4 has the same log and curves for well OCT-A2B. Figure 5 has

the same log and curves for well OCT-B6. Figure 6 has the same log and curves for well OCT-K5.

Table 3 Average formation evaluation parameters

Well/ Property	V_{sh} (%)	Ø (%)	$S_{w\ (\%)}$	Gross (ft)	Net (ft)	N/G (%)
OCT-B8	0.196	0.134	0.364	495	457	0.92
OCT-K5	0.183	0.13	0.474	546	405	0.74
OCT-A2B	0.206	0.1555	0.422	539	519	0.96
OCT-B6	0.193	0.134	0.454	532	469	0.88

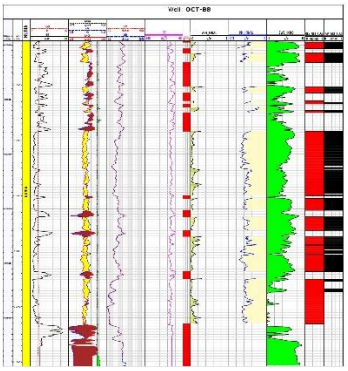

Figure 3 OCT-B8 formation evaluation, the Caliper log (CALI), Gamma Ray log (GR) are in the first track. Bulk Density log (RHOB), Neutron Porosity Log (NPHI) and Bulk Density Correction Log (DRHO) in the second track. The Deep Resistivity log (RD) and Medium Resistivity log (RM) in the third track. Sonic Travel Time log (DT) in the fourth track. Bad Hole Flag (BHF) in the fifth track, Final Shale Volume (V_{sh}) in the sixth track, Final Porosity (PHI_FINAL) in the seventh track and Indonesian (final) Water Saturation (SWE_INDO) in the eighth track. Finally, the Reservoir Net Flag (RES_NET_FLAG) exists in the ninth track and the Pay Net Flag (PAY_NET_FLAG) in the tenth track.

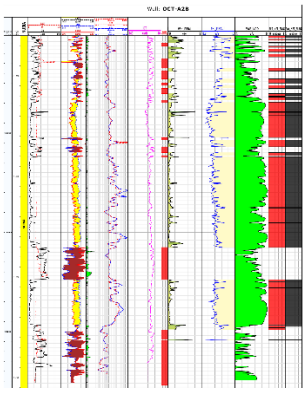

Figure 4 OCT-A2B formation evaluation, the Caliper log (CALI), Gamma Ray log (GR) are in the first track. Bulk Density log (RHOB), Neutron Porosity Log (NPHI) and Bulk Density Correction Log (DRHO) in the second track. The Deep Resistivity log (RD), Deep Induction Resistivity log (ILD), Medium Resistivity log (RM) and Medium Induction Resistivity log (ILM) in the third track. Sonic Travel Time log (DT) in the fourth track. Bad Hole Flag (BHF) in the fifth track, Final Shale Volume (V_{sh}) in the sixth track, Final Porosity (PHI_FINAL) in the seventh track and Indonesian (final) Water Saturation (SWE_INDO) in the eighth track. Finally, the Reservoir Net Flag (RES_NET_FLAG) exists in the ninth track and the Pay Net Flag (PAY_NET_FLAG) in the tenth track.

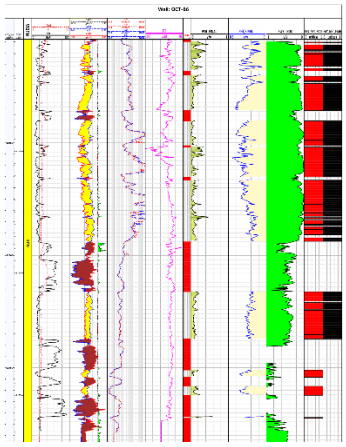

Figure 5 OCT-B6 formation evaluation, the Caliper log (CALI), Gamma Ray log (GR) are in the first track. Bulk Density log (RHOB), Neutron Porosity Log (NPHI) and Bulk Density Correction Log (DRHO) in the second track. The Deep Resistivity log (RD), Medium Resistivity log (RM) in the third track. Sonic Travel Time log (DT) in the fourth track. Bad Hole Flag (BHF) in the fifth track, Final Shale Volume (V_{sh}) in the sixth track, Final Porosity (PHI_FINAL) in the seventh track and Indonesian (final) Water Saturation (SWE_INDO) in the eighth track. Finally, the Reservoir Net Flag (RES_NET_FLAG) exists in the ninth track and the Pay Net Flag (PAY_NET_FLAG) in the tenth track.

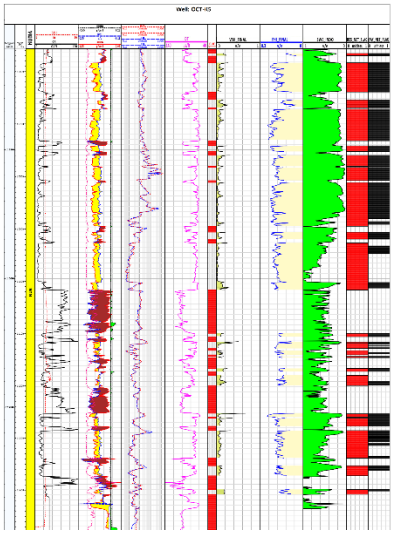

Figure 6 OCT-K5 formation evaluation, the Caliper log (CALI), Gamma Ray log (GR) are in the first track. Bulk Density log (RHOB), Neutron Porosity Log (NPHI), Photo Electric Effect Log (PEF) and Bulk Density Correction Log (DRHO) in the second track. The Deep Resistivity log (RD) and Medium Resistivity log (RM) in the third track. Sonic Travel Time log (DT) in the fourth track. Bad Hole Flag (BHF) in the fifth track, Final Shale Volume (V_{sh}) in the sixth track, Final Porosity (PHI_FINAL) in the seventh track and Indonesian (final) Water Saturation (SWE_INDO) in the eighth track. Finally, the Reservoir Net Flag (RES_NET_FLAG) exists in the ninth track and the Pay Net Flag (PAY_NET_FLAG) in the tenth track.

Mapping of petrophysical parameters for lateral variation

Mapping of petrophysical parameters shown a trend of loops with Northwest-Southeast direction where the enhanced petrophysical parameters are possibly located as the porosity increases and the shale volume decreases through this trend. Figure 7 shows the mapping of the average porosity of the area while Figure 8 shows the mapping of the average shale volume of the area.

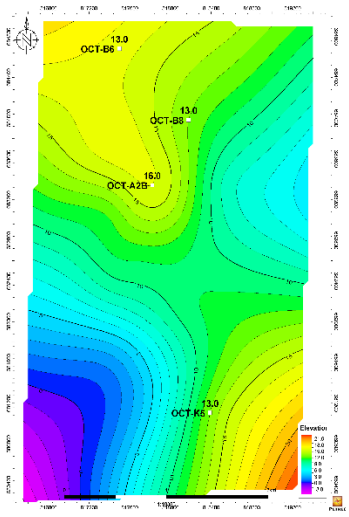

Figure 7 Average porosity mapping within the area

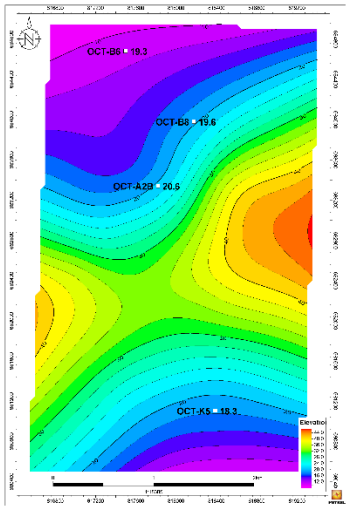

Figure 8 Average shale volume mapping within the area

Petrohysical parameters relations investigation

After the routine core analysis tests were done and data of porosity (COPHI) in percentage (%), horizontal permeability (COHK) in milli Darcy (mD), vertical permeability (COVK) in milli Darcy (mD) and core grain density (COGRD) in gram per cubic centimeter (g/cc) were obtained, some observations were done. This step aimed to explore the data through plotting some RCAL results versus each other and versus measured depth (MD) to search for any relations of insights that might benefit the study. This lead to six figures: Figure 9, Figure 10, Figure 11, Figure 12, Figure 13 and Figure 14, they are as following:

1- Horizontal permeability versus depth: Contradicting to the common, the horizontal permeability in chunks of the data increased with increasing depth.

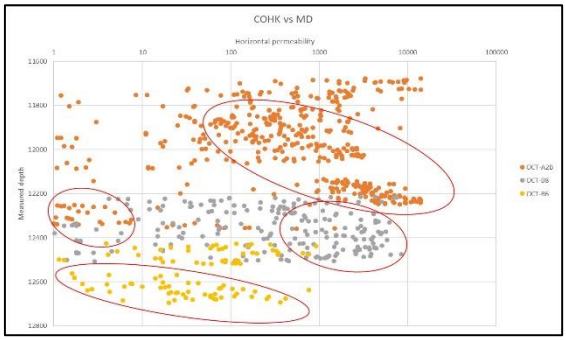

Figure 9 Horizontal permeability versus depth

2- Vertical permeability versus depth: Similarly, The vertical permeability performs in the same manner and gives the same anomalous trends in almost the same intervals.

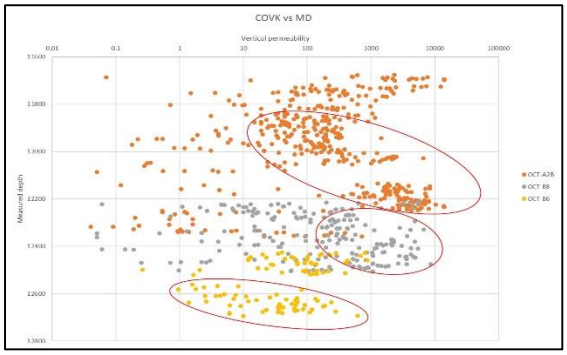

Figure 10 Vertical permeability versus depth

3- Core helium porosity versus depth: Similarly, the helium porosity performs in the same manner and gives the same anomalous trends in almost the same intervals.

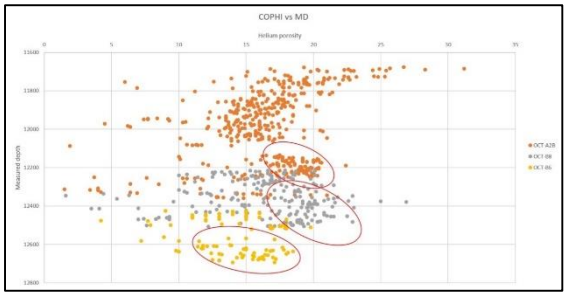

Figure 11 Helium porosity versus depth

4- Horizontal permeability versus vertical permeability: The horizontal and vertical permeability share an almost linear relation. This indicates the homogeneity of the Nubia Formation as permeability in all directions is similar.

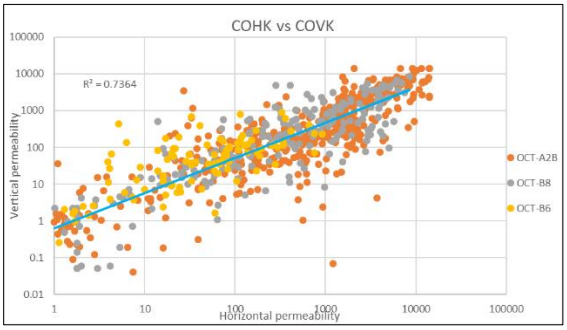

Figure 12 Horizontal permeability versus vertical permeability

5- Core helium porosity versus horizontal permeability: Similarly, the helium porosity is directly proportional with the horizontal permeability, it is also almost linear relation yet more scattered and less correlated. From the fitting line empirical equation (y= $0.279e^{0.4189x}$) where y is the horizontal permeability and x is the core helium porosity, the horizontal permeability could be estimated in un-cored intervals. The average horizontal permeability for the wells OCT-A2B, OCT-B8, OCT-B6 and OCT-K5 were 1326,930,451 and 610 milli Darcy respectively.

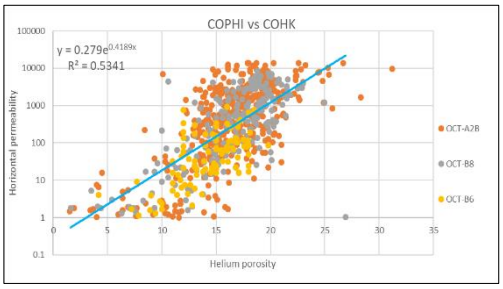

Figure 13 Helium porosity versus horizontal permeability

6- Core helium porosity versus vertical permeability: The helium porosity is directly proportional with the vertical permeability similar to that of helium porosity with horizontal permeability. From the fitting line empirical equation (y= $0.1291e^{0.4392x}$) where y is the vertical permeability and x is the core helium porosity, the vertical permeability could be estimated in un-cored intervals. The average vertical permeability for the wells OCT-A2B, OCT-B8, OCT-B6 and OCT-K5 were 975,683,309 and 431 milli Darcy respectively.

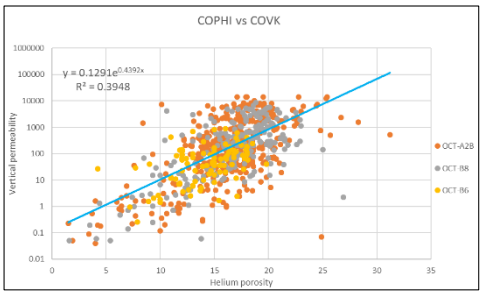

Figure 14 Helium porosity versus vertical permeability

Figures 15, 16, 17 and 18 show the horizontal and vertical permeability curves obtained from the empirical equations for the wells OCT-B8, OCT-A2B, OCT-B6 and OCT-K5 respectively. The first track contains the porosity calculated from the logs, the second track contains the calculated horizontal permeability curve along with the measured horizontal core permeability while the third track contains the calculated vertical permeability curve along with the measured vertical core permeability except for well OCT-K5 as it has no core.

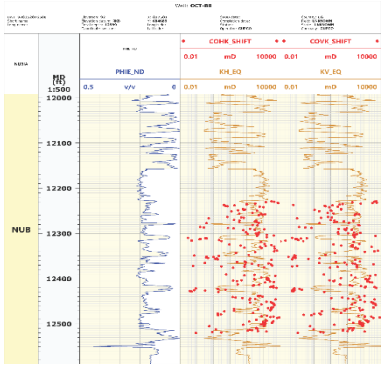

Figure 15 Calculated horizontal and vertical permeability curves from empirical equations for OCT-B8 well

 DOI: 10.21608/jpme.2024.275167.1192

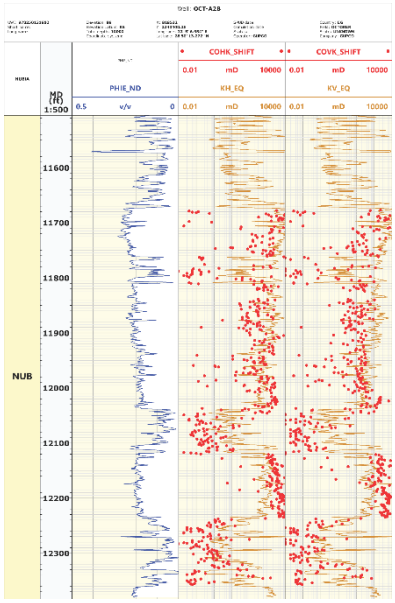

Figure 16 Calculated horizontal and vertical permeability curves from empirical equations for OCT-A2B well

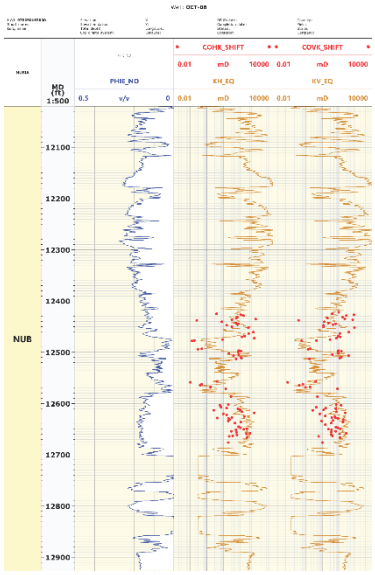

Figure 17 Calculated horizontal and vertical permeability curves from empirical equations for OCT-B6 well

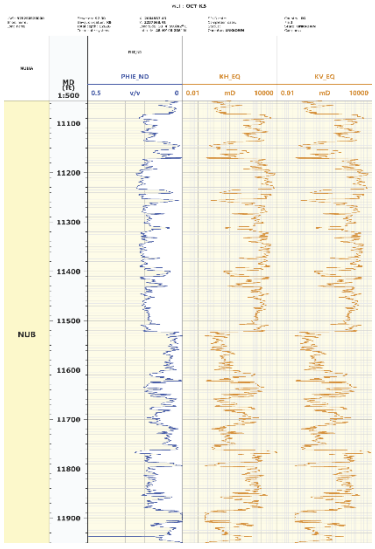

Figure 18 Calculated horizontal and vertical permeability curves from empirical equations for OCT-K5 well

Figure 19 and figure 20 shows a comparison of the calculated horizontal and vertical permeability from empirical equations versus the measured core horizontal and vertical permeability from core for the studied wells. As it is noticed there is a very weak to no correlation between the calculated permeability from empirical equations and measured permeability from core as the R2 correlation coefficient is 0.0296 in case of horizontal permeability comparison and 0.2108 in case of vertical permeability comparison. This is due the difference in porosity measured from core and porosity calculated from logs due to different measurement conditions such as the formation temperature and pressure, the well-hole condition, the mud effects, overburden pressure etc.

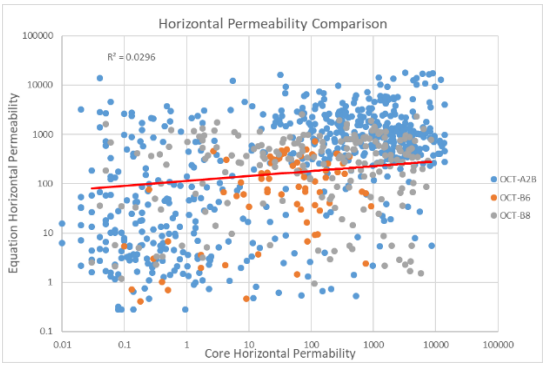

Figure 19 Comparison between calculated and measured horizontal permeability

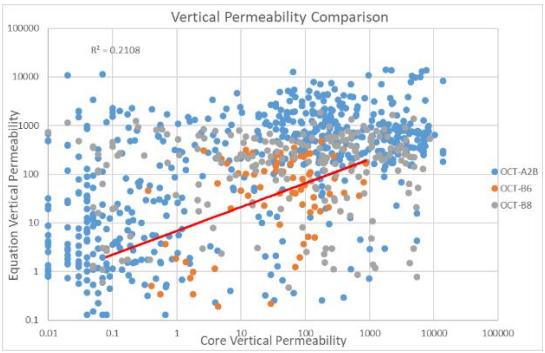

Figure 20 Comparison between calculated and measured vertical permeability

Conclusions

Shale volume ranges between about 18 and 20 percent in Nubia Formation in October field. Porosity ranges between about 13 and 16 percent in Nubia Formation in October field. Water saturation ranges between about 36 and 47 percent in Nubia Formation in October field. Nubia Formation is a good reservoir and net pay thickness ranges between 74 and 96 percent of the gross thickness. The helium porosity measured from core samples contradicts the common relation with depth in some intervals of the formation as it increases with the increasing depth. Helium porosity, horizontal permeability and vertical permeability are highly correlated with each other in the Nubia Formation. Porosity and permeability values from routine core analysis are plotted where empirical equations are deducted then utilized to

predict permeability in un-cored intervals. The average horizontal permeability ranged from 451 to 1326 mD while the range for vertical permeability was from 309 to 975 mD. This method resulted in low to very low R^2 correlation coefficient resulted as the comparison of actual and predicted horizontal permeability had an R^2 of 0.03 while the R^2 reached 0.21 in case of vertical permeability. Most important result is the knowledge acquired of the direction trend where enhanced petrophysical parameters are probably located, as loops with Northwest-Southeast direction were found with increased porosity and decreased shale volume. These results lead to reliable opportunities for delivering exploration and development wells to optimize the production of oil in the field as the results indicate massive hydrocarbon quantities.

Nomenclature

Mathematical term	Definition	Unit
a	Archie Constant	Unit-less
GR_{log}	Gamma ray log reading	API
GR_{sand}	Gamma ray log reading for clean and sand matrix	API
GR_{shale}	Gamma ray log reading for shale	API
k	Horizontal permeability	mD
$NPHI_{ma}$	Neutron log reading for clean matrix	Ratio
NPHI	Neutron log reading	Ratio
$NPHI_{sh}$	Neutron log reading for shale	Ratio
$NPHI_{fl}$	Neutron log reading for drilling fluid	Ratio
m	Cementation exponent	Unit-less
n	Saturation exponent	Unit-less
$RHOB_{ma}$	Density log reading for clean matrix	g/cc
RHOB	Density log reading	g/cc
$RHOB_{sh}$	Density log reading for shale	g/cc
$RHOB_{fl}$	Density log reading for drilling fluid	g/cc
R_W	Resistivity of formation water	Ohm.m
R_T	Resistivity of uninvaded formation	Ohm.m
S_W	Water saturation	Ratio
SW_{indo}	Indonesian water saturation	Ratio
Ø	Formation porosity	Ratio
Ø	Porosity measured from core	Ratio
$Ø_N$	Porosity derived from neutron log	Ratio
$Ø_D$	Porosity derived from density log	Ratio
$Ø_{sh}$	Porosity of shale derived	Ratio
$Ø_e$	Effective porosity	Ratio
$Ø_t$	Total porosity	Ratio
?	Density log reading	g/cc
ρ_{ma}	Density of the rock matrix	g/cc
ρ_{fluid}	Density of drilling fluid	g/cc
ρ_{log}	Density log reading	g/cc

Acronyms

Core Horizontal Permeability	COHK
Core Porosity	COPHI
Core Vertical Permeability	COVK
Barrel Oil Per Day	BOPD
Caliper Log	CALI
Deep Resistivity Log	RD
Density Log	RHOB
Gamma Ray	GR
Gulf Of Suez Petroleum Company	GUPCO
Medium Resistivity	RM
Million Barrel Oil	MMBO
Net To Gross Ratio	N/G
Neutron Log	NPHI
Oil Water Contact	OWC
Porosity	Ø
Routine Core Analysis	RCAL
Shale Volume	V_{sh}
Sonic Log	DT
Special Core Analysis	SCAL
True Vertical Depth Sub Sea	TVDSS
Water Saturation	S_w

Funding Sources

This research received no external funding.

Conflicts of Interest

There are no conflicts to declare.

Acknowledgements

The Authors would like to thank the Egyptian General Petroleum Corporation (EGPC) and Gulf of Suez oil company (GUPCO) for supplying the data for this study.

Notes and References

[1] Egyptian General Petroleum Corporation (EGPC), 1996. Gulf of Suez oil fields (a comprehensive overview). EGPC, Cairo, Egypt.

[2] Zahran, M., 1986. In Geology of October field, in: The 8th Exploration International Conference, Egyptian General Petroleum Cooperation, Cairo.

[3] Kassem, A.A., Sen, S., Radwan, A.E., Abdelghany, W.K., and Abioui, M., 2021. Effect of depletion and fluid injection in the Mesozoic and Paleozoic sandstone reservoirs of the October Oil Field, Central Gulf of Suez Basin: Implications on drilling, production and reservoir stability. Natural Resources Research, 30, 2587–2606.

[4] Khattab, M.A., Radwan, A.E., El-Anbaawy, M.I., Mansour, M.H., and El-Tehiwy, A.A., 2023. Three-dimensional structural modelling of structurally complex hydrocarbon reservoir in October Oil Field, Gulf of Suez, Egypt. Geological Journal.

[5] Elsayed, A.G., Kassab, M., and Osman, W., 2021. Evaluation of Petrophysical and Hydrocarbon Potentiality for the Nubia A, Ras Budran oil field, Gulf

of Suez, Egypt. Egyptian Journal of Chemistry, 64, 3387–3404.

[6] El Nady, M.M., Ramadan, F.S., Hammad, M.M., and Lotfy, N.M., 2015. Evaluation of organic matters, hydrocarbon potential and thermal maturity of source rocks based on geochemical and statistical methods: Case study of source rocks in Ras Gharib oilfield, central Gulf of Suez, Egypt. Egyptian Journal of Petroleum, 24, 203–211.

[7] Bosworth, W. and McClay, K., 2001. Structural and stratigraphic evolution of the Gulf of Suez rift, Egypt: a synthesis. Mémoires du Muséum national d'histoire naturelle, 186, 567–606.

[8] Moustafa, A.M., 1976. Block faulting in the Gulf of Suez, in: Proceedings of the 5th Egyptian General Petroleum Corporation Exploration Seminar, Cairo, Egypt.

[9] Patton, T.L., Moustafa, A.R., Nelson, R.A., and Abdine, S.A., 1994. Tectonic evolution and structural setting of the Suez rift: chapter 1: Part I. Type basin: Gulf of Suez.

[10] El-Ghamri, M.A., Warburton, I.C., and Burley, S.D., 2002. Hydrocarbon generation and charging in the October Field, Gulf of Suez, Egypt. Journal of Petroleum Geology, 25, 433–464.

[11] Radwan, A.E., Trippetta, F., Kassem, A.A., and Kania, M., 2021. Multi-scale characterization of unconventional tight carbonate reservoir: Insights from October oil field, Gulf of Suez rift basin, Egypt. Journal of Petroleum Science and Engineering, 197, 107968.

[12] Lelek, J.J., Shepherd, D.B., Stone, D.M., and Abdine, A.S., 1992. October Field: The Latest Giant under Development in Egypt's Gulf of Suez: Chapter 15.

[13] Radwan, A.E., Kassem, A.A., and Kassem, A., 2020. Radwany Formation: A new formation name for the Early-Middle Eocene carbonate sediments of the offshore October oil field, Gulf of Suez: Contribution to the Eocene sediments in Egypt. Marine and Petroleum Geology, 116, 104304.

[14] Borling, D.C., Powers, B.S., and Ramadan, N., 1996. Water Shut-Off Case History Using Through-Tubing Bridge Plugs; October Field, Nubia Formation, Gulf of Suez, Egypt, in: Abu Dhabi International Petroleum Exhibition and Conference. OnePetro.

[15] Hussein, I., El Kammar, A.M., Maky, A.F., and Elshafeiy, M., 2017. Comparative organic geochemical studies on some Miocene and Cretaceous rock units in October field, Gulf of Suez, Egypt.

[16] Peijs, J., Bevan, T.G., and Piombino, J.T., 2012. The Gulf of Suez rift basin, in: Regional Geology and Tectonics: Phanerozoic Rift Systems and Sedimentary Basins. Elsevier, pp. 164–194.

[17] Deaf, A.S., 2009. Palynology, palynofacies and hydrocarbon potential of the Cretaceous rocks of northern Egypt. University of Southampton.

[18] Hasouba, M., Abd El Shafy, A., and Mohamed, A., 1992. Nezzazat Group—reservoir geometry and rock types in the October field area, Gulf of Suez, in: 11th EGPC Petroleum Exploration and Production Conference, pp. 293–317.

[19] El-Ghamri, M.A., Warburton, I.C., and Burley, S.D., 2002. Hydrocarbon generation and charging in the October Field, Gulf of Suez, Egypt. Journal of Petroleum Geology, 25, 433–464.

[20] Atlas, D., 1979. Log Interpretation Charts. Dresser Industries. Inc., 107 p.

[21] Schlumberger, L.I., 1972. Volume 1-Principles. Schlumberger Limited, New York, 113.

[22] Schlumberger, E.U.M., 2009. Technical description. Schlumberger Ltd, pp. 519–538.

[23] Wyllie, M.R.J., 1963. The fundamentals of well log interpretation. Academic Press.

[24] Asquith, G.B. and Gibson, C.R., 1982. Basic well log analysis for geologists. American Association of Petroleum Geologists, Tulsa.

[25] Poupon, A. and Leveaux, J., 1971. Evaluation of water saturation in shaly formations, in: SPWLA 12th Annual Logging Symposium. OnePetro.

[26] Darling, T., 2005. Well logging and formation evaluation. Elsevier.

[27] Kassab, M.A., Abbas, A., and Ghanima, A., 2020. Petrophysical evaluation of clastic Upper Safa Member using well logging and core data in the Obaiyed field in the Western Desert of Egypt. Egyptian Journal of Petroleum, 29, 141–153.

[28] El-Din, E.S., Mesbah, M.A., Kassab, M.A., Mohamed, I.F., Cheadle, B.A., and Teama, M.A., 2013. Assessment of petrophysical parameters of clastics using well logs: The Upper Miocene in El-Wastani gas field, onshore Nile Delta, Egypt. Petroleum Exploration and Development, 40, 488–494.

[29] Kassab, M.A., Abbas, A.E., Osman, I.A., and Eid, A.A., 2024. Reservoir rock typing for optimum permeability prediction of Nubia formation in October Field, Gulf of Suez, Egypt. Journal of Petroleum Exploration and Production Technology, pp. 1–22.